Image charge force of keV ions through insulating nanocapillaries

Eric Giglio

Image charge force of keV ions through insulating nanocapillaries

Eric Giglio
Centre de Recherche sur les Ions, les Matériaux et la Photonique,
Normandie Université, ENSICAEN, UNICAEN, CEA, CNRS, F-14000 Caen, France

(Received 4 September 2022; accepted 3 January 2023; published xxxxxxxxxx)

In nanocapillaries of large aspect ratio, the attractive image charge force is strong enough to affect the trajectory of ions passing through capillaries and consequently to diminish the fraction of transmitted beam ions. We calculated the theoretically transmitted fraction, using an expression of the image charge force valid in the case of a static ion and an infinite cylindrical dielectric interface. When comparing the theoretically transmitted fraction to the available experimental data for nanocapillaries with an inner diameter of less than 200 nm, we found a surprisingly large disagreement, i.e., the theoretically transmitted fractions were easily an order of magnitude lower than the experimental ones. Noting that the image charge force depends on the velocity of the ion via the frequency-dependent relative permittivity of the insulator, we investigated whether the disagreement could be lifted using a velocity depend image charge force. We give the exact expressions of the dynamical image charge force for a plane and cylindrical dielectric interface as a function of the ion velocity. We then reevaluated the theoretically transmitted fractions in the case of SiO_2 and polyethylene terephthalate dielectric interfaces. Our findings are discussed in light of the available experimental data.

DOI: 10.1103/PhysRevA.00.002800

I. INTRODUCTION

Guiding of low-energy ions by insulating capillaries was first reported by Stolterfoht *et al.* in 2002 for nanocapillaries [1] and later by Ikeda *et al.* [2] for macroscopic glass capillaries. Their experimental results showed that even though the capillaries were tilted with respect to the beam axis, such as no geometrical transmission being allowed, the beam was steered after an initial charge-up phase through the insulating capillary by self-organized charge patches. As a result, a part of the beam could be transmitted, with the ions keeping their initial charge state, indicating that the ions never touched the inner wall. Those pioneering results triggered numerous experimental and theoretical studies allowing a better understanding of the guiding process of keV ions through insulating capillaries [3,4]. For an overview, see [5,6]. By combining available experimental data with theoretical predictions, insulating capillaries became a formidable tool to explore the dynamics of excess charges in insulators in the presence or absence of charge injection. Indeed, the time-evolution of the rate, energy, and angular profile of the transmitted ions may give indirectly information about the relaxation process of excess charge in insulating capillaries and even about the charge injection process by ion-surface collisions.

Over time, models for the charge dynamics in insulating capillaries were contentiously refined to improve the description of the charge injection and charge relaxation in insulating capillaries [7–12]. In particular, the electric field inside the capillary was calculated precisely by considering the appropriate boundary conditions at the inner and outer surfaces of the capillary [9]. In recent models for glass macrocapillaries, the charge injection at the inner surface term accounts even for secondary electrons emitted by ion-surface collisions and subsequently reabsorbed by the surface [11]. In nanocapillaries, the bulk and surface currents were even considered to depend nonlinearly on the electric field as the electric field in nanocapillaries easily exceeded the keV/mm [8]. Eventually, the image charge force acting on the beam ions inside nanocapillaries was added to the dynamics to explain the observed beam-shaping of transmitted ions through muscovite mica nanocapillaries with rhombic and rectangular sections [13,14]. Indeed, when an ion approaches a dielectric interface separating two different dielectric media, the induced surface polarization charges attract the ion toward the interface. In nanocapillaries, the attractive image charge force was shown to be strong enough to sensibly affect the trajectory of passing ions, and consequently, the fraction and angular distribution of transmitted beam ions.

In this work, we propose taking a closer look at the modeling of the image charge force acting on beam ions through cylindrical nanocapillaries. In particular, we want to investigate whether experimentally observed transmission rates through insulating straight nanocapillaries are well reproduced using the expression of the image force inside a cylindrical dielectric. Several experimental studies reported the transmission rates of keV ions through insulating nanocapillaries [4,13,15,16]. Here, we are mostly interested in those cases where a uniform keV ion beam was injected at zero tilt angle and for which the measured transmitted fraction, defined as the transmitted current divided by the injected current, was given. These experimental conditions constitute an ideal setup for which the transmitted fraction can be calculated analytically as the ion trajectories are dominated by the image charge force. Indeed, as will be discussed further in the text, for a uniform beam, aligned with the capillary axis, the charge deposited in the capillary is axisymmetric, yielding

an inner radial electric field that is negligible compared to the image charge force. As a result, ion beams through zero-tilted nanocapillaries are a formidable tool to investigate the image force of ions moving along a cylindrical dielectric interface.

The paper is organized as follow. In Sec. II, we propose and discuss a closed and accurate formula that fits the exact image force of a charge sitting inside a cylindrical dielectric interface. We then calculate the theoretical transmitted fraction in the case where the injected beam is aligned with the capillary axis. Next, we highlight the discrepancy between the theoretical and the experimental transmitted fractions found in the literature. That finding made us question the validity of the expression of the image charge force used here. In Sec. III we propose to improve the expression of the image charge force by explicitly taking into account the velocity of the ion and the frequency dependence of the relative permittivity of the capillary. We then calculate the image charge force as a function of the ion velocity and discussed its influence in the case of an arbitrary dielectric response function. In Sec. IV we reevaluate the theoretical transmitted fractions using this time the velocity-dependent image charge force, mainly for those cases for which experimental data are available in the literature. We discuss then in how far the velocity-dependent image charge force lifts the initially mentioned discrepancy.

II. THEORETICAL AND EXPERIMENTAL TRANSMITTED FRACTIONS

The ion trajectories through a capillary is affected by two fields, the electric field generated by the accumulated charges in the capillary wall and by the image force. First, we show that, in the case where a keV ion beam is injected with zero tilt angle into a straight insulating nanocapillary, the transmitted beam fraction is mainly controlled by the image force, while the deposited charge has no notable effect on the transmission.

Indeed, for a beam aligned with the capillary axis, the deposited charge distribution has axial symmetry, generating an axisymmetric electric potential $V(\rho,z)$. Such a potential yields an inner electric field that competes with the image force only if the accumulated charge density in the bulk exceeds a certain amount. However, because the insulator cannot withstand an electric field larger than the dielectric strength field, typically 50 kV/mm [17], without undergoing electrical breakdown and becoming electrically conducting, the accumulated charge in the capillary wall is limited. We performed simulations with our numerical code INCA4D [10] where we followed the trajectories of 7-keV ions through a SiO_2 nanocapillary. Expression (6), which will be discussed later in the text, was used for the image force. We monitored the ion transmission for several hours (see black curve in Fig. 1) and found that the transmission is stable in time and neither increased nor reduced by the deposited self-organized charge. Details of the calculations are presented in Appendix A 1. Simulations confirm that the effect of the deposited charge on the transmission is negligible and that it is not possible to charge an insulating nanocapillary to the necessary amount to generate an inner electric field that competes with the image force. We can thus safely assume that the transmitted fraction is exclusively controlled by the image force.

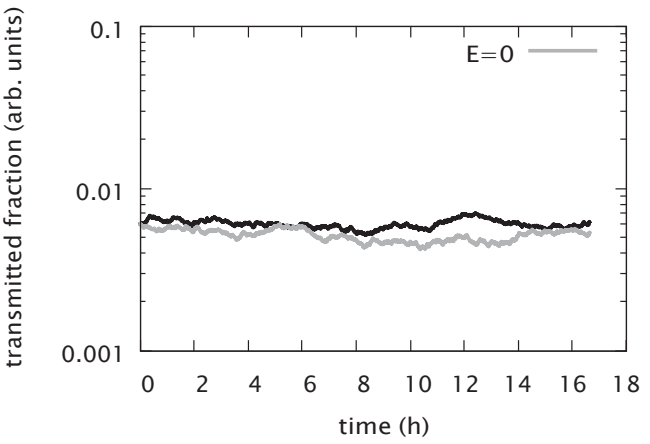

FIG. 1. Simulated transmitted beam fractions (black curve) through an insulating nanocapillary. The gray curve, for which the electric filed due to deposited charges was removed, is added for comparison.

A. Image charge force at a cylindrical dielectric interface

Let us assume a translationally invariant cylindrical dielectric interface of radius R, separating the inner vacuum from the outer insulating medium of dielectric relative permittivity $\varepsilon_r > 1$. A charge q is located inside the cylinder at position $\rho < R$, where ρ is the distance from the symmetry axis Oz. The modeling of the image force acting on the charge q is described in detail in [18–20]. Using cylindrical coordinates (ρ, θ, z) and introducing the dimensionless radial component

$$e = \rho/R,$$

the resulting force is given as a sum over angular moments m and dimensionless wave numbers k,

$$F_{\rm im}(e) = \frac{q^2}{16\pi\epsilon_0 R^2} \int_0^\infty dk\, A_m(k,\varepsilon_r)\, \frac{\partial I_m^2(ke)}{\partial e}\, u_\rho, \qquad (1)$$

where u_ρ is the radial unit vector, $I_m()$ the modified Bessel function of order m, and $A_m()$ a dimensionless function, accounting for the dielectric permittivity ϵ_r of the capillary. The expression of $A_m()$ is given by Eq. (14). Because of the sum over m and k, computing the image charge force $F_{\rm im}$ may be quite time consuming in simulations and a computationally faster expression approaching $F_{\rm im}$ would be welcomed. In the case of a perfectly conducting cylindrical interface, Tőkési *et al.* approached expression (1) by the closed expression of the image force of a charge inside a conducting sphere [18–21]. Extending that idea to a dielectric interface, we propose to approach $F_{\rm im}$ in a first step by the leading (zero-order) term of the image force of a charge inside a dielectric sphere, see Appendix A 3,

$$F^\circ_{\rm im}(e) = \frac{q^2}{4\pi\epsilon_0 R^2}\,\frac{\epsilon_r - 1}{\epsilon_r + 1}\,\frac{e}{(1-e^2)^2}\,u_\rho. \qquad (2)$$

To check how well $F^\circ_{\rm im}$ approaches $F_{\rm im}$, we compute the ratio $F_{\rm im}/F^\circ_{\rm im}$ as a function of e and for various values of ε_r. Interestingly, the ratio $F_{\rm im}/F^\circ_{\rm im}$ is independent of R as both $F_{\rm im}(e)$ and $F^\circ_{\rm im}(e)$ scale as R^{-2}. The ratio can thus be evaluated for arbitrary R. Here, $F_{\rm im}(e)$ is evaluated using $R = 1$ and

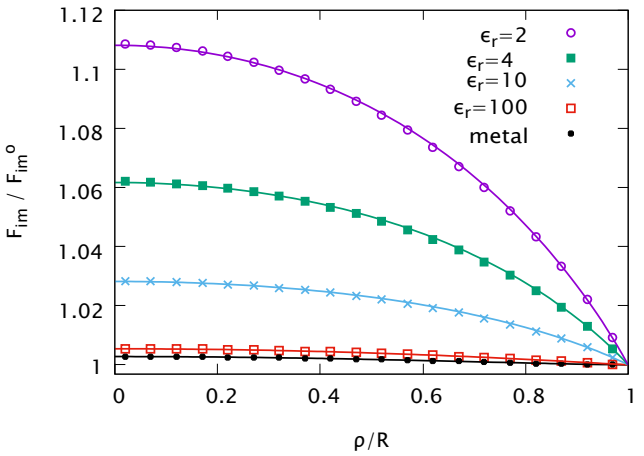

FIG. 2. Ratio $F_{\rm im}/F^0_{\rm im}$ as a function of ρ/R for various ε_r. The label "metal" stands for a perfectly conducting interface. The full curves are the function $h_{\varepsilon_r}(\rho/R)$ for $\varepsilon_r = 2, 4, 10, 100$ and $|\varepsilon_r| \to \infty$.

the sum over m is limited to the first 200 angular moments, which is found to be sufficient for an accurate evaluation of Eq. (1) up to a radial position $e \leq 0.98$. Results are shown in Fig. 2 for a selection of ε_r. We see that the ratio gets globally closer to the unit with increasing ε_r. In addition, for a perfectly conducting cylindrical interface, $|\varepsilon_r| \to \infty$, the ratio lies between 1.0027 and 1. Predictably, the deviation is systematically larger for a charge located close to the symmetry axis ($e \ll 1$), but even for $\varepsilon_r = 2$, the relative deviation in that case is only about 11%. Importantly, close to the interface, $e \to 1$, $F^\circ_{\rm im}$ tends asymptotically to $F_{\rm im}$. Indeed for $\rho \gg R$, the cylindrical and spherical interfaces can both be assimilated by a plane interface and their expressions yield the same limit, namely, that of the image force (12) of a plane surface. We thus deduce that the exact expression $F_{\rm im}$ is surprisingly well approached by $F^\circ_{\rm im}$, considering that the curvatures of the cylindrical and spherical interfaces are different. In addition, $F^\circ_{\rm im}$ is less precise where the force is still relatively weak.

Obviously, an even better fit for Eq. (1) can be found. Looking at the data in Fig. 2, we notice that all five ratios deviate from the unit in a scaled manner. We find that those ratios are well fitted by a function of the form

$$h_{\varepsilon_r}(e) = 1 + \alpha(1 - e^2) + \beta(1 - e^2)^{3/2}, \tag{3}$$

where α and β are parameters depending on ε_r. Checking for a large selection of $\varepsilon_r \geq 2$, we find that the relation between α, β, and ε_r can be written in the form

$$\alpha = 0.48/(\varepsilon_r + 1), \tag{4}$$

$$\beta = 0.00278 - 0.22/(\varepsilon_r + 2). \tag{5}$$

We superimposed the data in Fig. 2 to the function $h_{\varepsilon_r}(e)$ with corresponding ε_r. The excellent agreement (a relative error of less than 5×10^{-4}) indicates that the closed formula

$$F^{\rm cyl}_{\rm im}(e) = F^\circ_{\rm im}(e) \times h_{\varepsilon_r}(e), \tag{6}$$

with h_{ε_r} defined by Eqs. (3), (4), and (5) is an excellent approximation to the exact image force (1) for a cylindrical dielectric interface. In simulations for which the computational cost for the evaluation of the image force is critical, we can safely suggest the closed formula (6) instead of the exact but CPU consuming expression (1).

B. Ion trajectories and the theoretical transmitted fraction

We will now define the theoretically transmitted fraction $f_{\rm th}$ of an injected ion beam at zero tilt angle in the ideal case where the capillary is a straight tube and the uniform, monokinetic ion beam has zero divergence. We assume that a charge q of mass m and energy E_k enters the cylindrical capillary with an initial radial distance $\rho_0 < R$ and with an initial velocity $v_0 = \sqrt{2E_k/m}\,u_z$, so that at $z = 0$ we have $d\rho/dz = 0$.

The theoretically transmitted fraction $f_{\rm th}$ is evaluated using $F^\circ_{\rm im}$ because the latter allows to establish a simple but useful relation between $f_{\rm th}$ and the properties of the capillary and the ion beam. We further check that using the more precise formula $F^{\rm cyl}_{\rm im}$ introduces only a negligible correction to $f_{\rm th}$, giving confidence in the present approach.

The trajectory $\rho(z)$ of the ion can then be readily computed by solving the differential equation

$$\frac{d^2\rho}{dz^2} = \frac{1}{2E_k} F^\circ_{\rm im}[\rho(z)/R], \tag{7}$$

with the initial values $\rho(0) = \rho_0$ and $\frac{d\rho}{dz}|_{z=0} = 0$. Using the dimensionless quantities $e = \rho/R$ and $\zeta = z/H$, Eq. (7) can be rewritten in dimensionless form

$$\frac{d^2 e}{d\zeta^2} = \Gamma \frac{e(\zeta)}{[1 - e(\zeta)^2]^2}, \tag{8}$$

with $e_0 = \rho_0/R$ and $\frac{de}{d\zeta}|_{\zeta=0} = 0$ and where the dimensionless factor

$$\Gamma = \frac{q^2}{4\pi\varepsilon_0} \frac{\varepsilon_r - 1}{\varepsilon_r + 1} \frac{1}{2E_k} \frac{H^2}{R^3} \tag{9}$$

accounts for the length H, inner radius R, and dielectric constant ε_r of the capillary as well as the kinetic energy E_k of the charge. Remarkably, the factor Γ tells us that the dimensionless image charge force scales with the square of the capillary length H and with the inverse cube of the capillary radius R. This explains why, for nano and macrocapillaries of the same aspect ratio H/R, the force can be neglected in macrocapillaries ($R \sim 1$ mm) but not in nanocapilleries ($R \sim 100$ nm). Also, note that the force is inversely proportional to the kinetic energy of the ions.

Equation (8) is solved numerically, using a standard fourth-order Runge-Kutta method. For a given Γ and for a given initial value e_0 the trajectory $e(\zeta)$ is uniquely defined. If the trajectory is intercepted by the capillary wall, we reduce the initial value of e_0, otherwise e_0 is increased. Using the bisection method, a good estimate for the largest value of $e_0^{\rm max}$ for which the ion is still transmitted is found. Assuming that the injected current density j_0 is uniform, we have $I_{\rm in} = j_0\pi R^2$ and $I_{\rm out} = j_0\pi(e_0 R)^2$. The ratio

$$\frac{I_{\rm out}}{I_{\rm in}} = e_0^{\rm max}(\Gamma)^2 = f_{\rm th}(\Gamma) \tag{10}$$

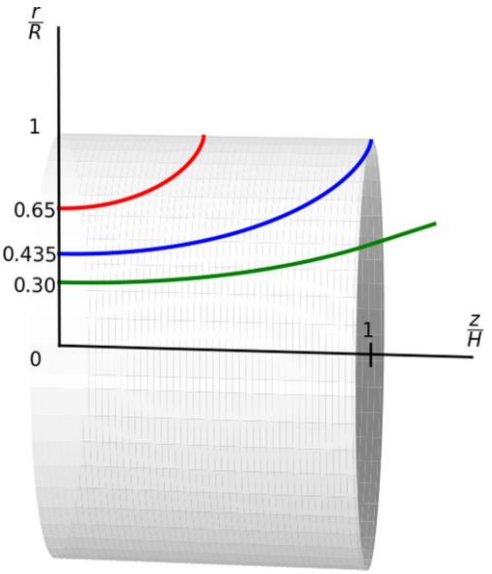

FIG. 3. Trajectories for three different initial values of ϵ_0 in the case of $\Gamma = 1$. Only for $\epsilon_0 < \epsilon_0^{max} = 0.435$ are the ions transmitted, so that, for $\Gamma = 1$, the transmitted fraction f_{th} equals $\epsilon^2 = 18.6\%$.

defines the theoretical transmitted fraction f_{th} of the ion beam in the ideal case where the nanocapillary is a straight cylinder and the ion beam has zero divergence. The fraction f_{th} depends only on the factor Γ and has to be understood as an upper bound value, obtainable only in ideal conditions, i.e., the injected beam is spatially uniform, monokinetic, parallel, and the capillary is perfectly cylindrical. In Fig. 3, we show three trajectories for three different values of r_0 in the case of $\Gamma = 1$. We see that only the ions that are injected at a distance less than $\epsilon_0^{max} = 0.435$ are transmitted, so that for $\Gamma = 1$ the transmitted fraction f_{th} equals 18.6%. The theoretical transmitted fraction was calculated for a large range of Γ and is shown in Fig. 4 by the full black curve. In the case of marcocapillaries, Γ is typically well below 10^{-4}, yielding f_{th} close to 100%. As expected, this indicates that the effect of the image charge force on the ion trajectory is negligible

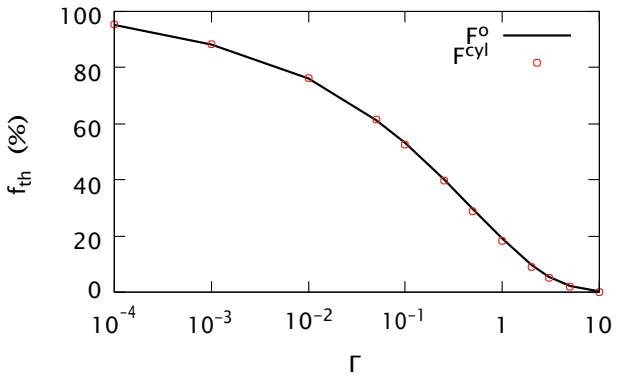

FIG. 4. Theoretical transmitted fraction f_{th} (in percentage) as a function of the dimensionless parameter Γ defined by Eq. (9) in the case of a uniform, divergence-less ion beam aligned with the capillary axis. Full black line is computed using F°_{im} while the red circles were obtained with $F^{cyl}_{im} = F^{\circ}_{im} \times h_{\varepsilon_r}$ and $\varepsilon_r = 2$.

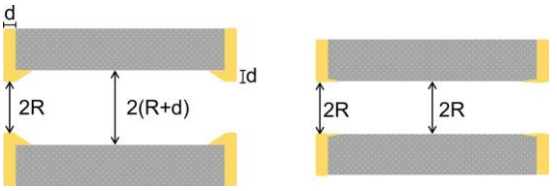

FIG. 5. Schematic representation of the presence (left) or absence (right) of a cold collar of thickness d at the inlet and outlet of a capillary after a gold deposition occurred on the front and back side of the insulating sheet containing the capillaries.

in macrocapillaries. However, for keV ions through nanocapillaries, Γ is of the order of the unit, and the ions transmission is expected to be strongly reduced by the image charge force. For Γ as large as 10, the transmitted fraction falls even below 1%. We add to Fig. 4 the values of f_{th} evaluated with F^{cyl}_{im} (red circles) instead of F°_{im}. We used F^{cyl}_{im} with $\varepsilon_r = 2$, which corresponds to the case where the correction h_{ε_r} is the largest. We note that the black curve tends to slightly overestimate f_{th} for larger Γ, but, in general, the difference with red circles is rather negligible, indicating that F°_{im} is already a good approximation for Eq. (1).

C. Comparison with experimental data

We can now compare the theoretically transmitted fraction to the one found in previously published works and discuss the observed discrepancies. This allows us to highlight a disagreement between the theoretical and experimentally observed transmitted fraction and of ions through nanocapillaries. Note that, for the following discussion, the more precise formula $F^{cyl}_{im}(\epsilon)$ is used to evaluate the theoretically transmitted fraction instead of $F^{\circ}_{im}(\epsilon)$.

In experimental works on nanocapillaries, authors usually gave the transmitted ion rate I_{out} through a large number of capillaries rather than the transmitted fraction I_{out}/I_{in}. Indeed, the injected ion rate I_{in} has to be deduced from the current density and size of the beam, as well as the transparency of the foil containing the capillaries, parameters which are difficult to obtain with sufficient precision. We nevertheless found three experimental studies which gave the transmitted fraction at zero tilt angle.

Surprisingly, when comparing the theoretical transmitted fractions f_{th} to the experimental data found in [4,15,16], we noticed a significant disagreement. In a recent work by Stolterfoht *et al.* [16], a transmitted fraction of 50% was observed for an 3-keV Ne^{7+} ion beam through polyethylene terephthalate (PET) nanocapillaries. These have a length of $H = 12$ μm and a diameter of $2R = 230$ nm. To avoid charge-up of the insulating film by the ion beam, a gold layer of about 20 nm was deposited on both sides. This may result in a gold collar reducing the inlet and outlet diameter of the nanocapillaries, see Fig. 5. The inlet and outlet diameters, as measured by scanning electron microscopy (SEM) after gold deposition, may thus underestimate the diameter of the capillary up to 40 nm. While we found no clear experimental evidence that showed that a collar of tens of nm thickness was present, we will nevertheless evaluate f_{th} for both cases, with and

without a 20-nm circular gold collar at the inlet and outlet of the capillaries. We specify that, for the gold deposition process, the capillaries were tilted by 30° with respect to the gold vapor and then turned by 180°. Accordingly, the collar may not be perfectly circular but rather some kind of ellipse. Nevertheless, for the present purpose we assume that the gold coverage has circular geometry.

Using for PET a dielectric constant of 3.0 [22], we have for the parameter Γ a value of 0.55. The theoretically transmitted fraction obtained for $\Gamma = 0.55$ is 27%, which is lower than the experimental one by almost a factor of 2. If we account for a 20-nm collar, $f_{\rm th}$ increases to 31%. To recover the experimental transmitted fraction of 50%, the parameter Γ needs to be reduced by a factor of 4. This can be achieved by reducing ε_r to 1.3, which yields, however, a nonphysically low value for ε_r. Alternatively, it can be achieved by increasing the diameter $2R$ of the capillaries by a factor of 1.5, that is, $2R$ 350 nm. But that would mean that the diameters measured by SEM underestimate the actual inner diameter of the capillaries by about 120 nm, which seems unlikely.

In 2010, Stolterfoht *et al.* measured the transmission rates of PET nanocapillaries of various diameter $2R_i$, ranging from 100 to 400 nm [15]. They did not give the transmitted fraction for each diameter but rather the relative transmitted ion yield. Obviously, this analysis advocates that, for those measurements, the current density and spot size of the injected ion beam was kept constant. The injected ion yield $I_{\rm in}$ can thus be considered proportional to the inlet section πR_i^2 of the capillaries.

$$I_{\rm in} \propto R_i^2.$$

Consequently, we find that the experimentally transmitted fraction $I_{\rm out}/I_{\rm in}$ is proportional to the transmitted ion yield divided by the inlet section

$$\frac{I_{\rm out}}{I_{\rm in}} \propto \frac{I_{\rm out}}{R_i^2}.$$

In Fig. 6, we compare $\propto I_{\rm out}/R_i^2$ to the theoretically transmitted fractions for the capillary diameters used in [15]. The proportionality factor was chosen such that $I_{\rm out}/I_{\rm in}$ coincides with $f_{\rm th}$ for capillaries with the largest diameter, namely $2R_i =$ 400 nm. We also add the fractions for $2R_i =$ 230 nm, discussed previously. We see that the experimentally transmitted fractions (red triangles) diminishes only slightly with decreasing $2R_i$. This is surprising because Eq. (9) tells us that Γ scales as R^{-3} and thus a strong dependence of the transmitted fraction on the capillary radius is expected, as shown in Fig. 4.

Our model predicts that $f_{\rm th}$ decays much faster with decreasing capillary diameter. In particular for $2R_i = 100$ nm, the discrepancy is huge. The theoretical transmitted fraction, without a collar, is 30 times smaller than the observed one. If we consider a 20-nm gold collar at the inlet and outlet of the capillaries (blue filled circles), $f_{\rm th}$ increases slightly, especially for smaller diameters. But even then, $f_{\rm th}$ is six times smaller than the experimental one for $2R_i = 100$ nm.

In their work of 2006 on highly ordered SiO_2 nanocapillaries, Sahana *et al.* [4] found that 20% of the Ne^{7+} ions, entering the capillaries at zero tilt angle, were being transmitted. They used a 7-keV ion beam and the nanocapillaries had a length of $H = 25$ μm and a diameter about $2R$ 100 nm, yielding a large aspect ratio of about $H/(2R)$ 250. A 30-nm gold layer was evaporated on both sides of the the film. Taking for the dielectric constant of amorphous SiO_2 a value of 3.9 [23], we obtain using Eq. (9) for the factor Γ a value of 14.9. For such a large Γ, our simulations find that only those ions which are injected within an initial distance $\rho \leq 2$ nm from the symmetry axis are transmitted. The theoretical transmitted fraction $f_{\rm th}$, calculated with $\Gamma = 14.9$ is 0.2%, is lower than the experimental one by a factor of 100. If we consider a 30-nm gold collar, $f_{\rm th}$ increases to 1%, which is still a factor of 20 from the experimental one. To recover the experimental transmitted fraction of 20%, the scaling factor Γ should be reduced here by a factor of 14. Either the transmitted fraction was overestimated by the authors, the measurement of the capillary diameter was underestimated, or the image force as given by Eq. (6) and thus Eq. (1) is not appropriate.

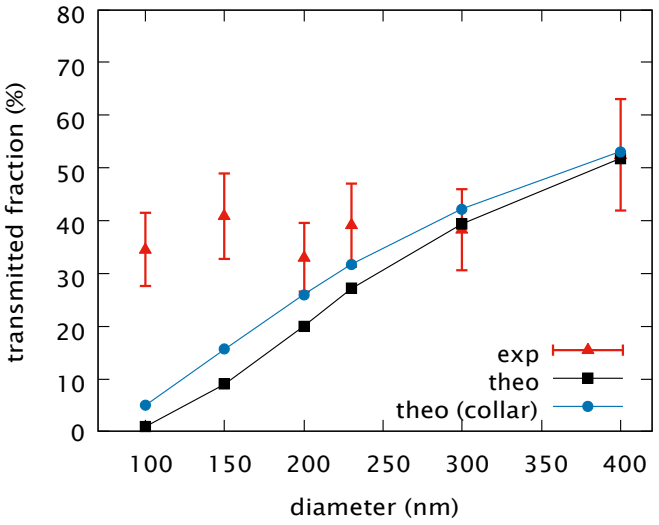

FIG. 6. Comparison between experimentally transmitted fractions (red triangles) extracted from [15,16] and our theoretically transmitted fractions as a function of the capillary diameter $2R_i$. Experimental data are normalized such that fractions coincides for capillaries with 400-nm diameter. Filled blue circles give the theoretically transmitted fractions in the case where the inlet and outlet diameters include a 20-nm collar, filled black squares are evaluated without collar.

The observed transmitted fractions in those three studies [4,15,16] were systematically significantly larger than those found theoretically in the ideal case. The experimental data do not corroborate the theoretical scaling of the transmitted fraction with the capillary radius. For keV ions, the intensity of the image force in cylindrical capillaries with a diameter smaller the 200 nm seems thus to be much lower than what was predicted theoretically. One possibility is that the image charge force expressed by $F_{\rm im}^{\rm cyl}(e)$ in Eq. (6) is not valid for keV ions through nanocapillaries. In addition, as Eq. (6) fits the exact expression $F_{\rm im}(e)$ extremely well, the same holds for $F_{\rm im}(e)$ in Eq. (1). We remind that expression (1) was obtained in the electrostatic limit with a static relative permittivity ε_r.

Case of rhombic and rectangular capillaries

Apart from cylindrical nanocapillaries, experimental studies were also done on muscovite mica nanocapillaries with the rhombic (long axis 248 nm and short axis 142 nm) and rectangular sections (215×450 nm^2) [13,14]. The observed beam-shaping of the transmitted ion was shown to be due to the image charge force, indicating clearly that the image charge force dominantly influences the ion trajectories. In their simulations, the image charge force is a superposition of the image charge force for a plane dielectric surface for each of the four plane surfaces. Interestingly, their simulations succeed in reproducing the observed transmitted fraction of about 1% for 7 keV Ne^{7+} through the rhombic-shaped muscovite mica nanocapillaries. However, in the case of rectangular capillaries, the simulated transmission rate and experimental values differ considerably (the experimental values are lower), but are attributed to size variations inside the channels.

We conclude this section by noting that significant disagreements were found between the measured and theoretical transmitted fractions in the case of cylindrical nanocapillaries made in PET and SiO_2. Better agreement was noticed in the case of rhombic-shaped mica nanocapillaries, but was not further confirmed in nanocapillaries with rectangular sections. Where disagreement was found, the experimentally transmitted fraction was always significantly larger than the simulated one.

III. VELOCITY-DEPENDENT IMAGE CHARGE FORCE

The disagreement highlighted in the previous section made us question the validity of expression (1) of the image charge force in the case where keV ions pass through a nanocapillary of the large aspect ratio. There are indeed two effects that we ignored in the evaluation of the image charge force $F_{\mathrm{im}}(\rho)$. If the inner surface of the capillary is hit by ions, the accumulated charge may modify the dielectric response of the insulator. For example, in precharged PET samples, the trapped charge was found to partially inhibit the dipolar polarization, reducing by about 5% the dielectric permittivity with respect to untreated PET [24]. However, except for the findings in [24], where the study was limitied below the 1-MHz domain, no other reference was found. So while the accumulated charge seems indeed to modify the dielectric response, the effect of excess charge on the dielectric response function is hardly documented in the literature and otherwise difficult to estimate by simple considerations. Thus, we decide for the present study to ignore the effect of the charge on the dielectric response.

The other effect is that the ions are moving and the velocity of the ions influences the induced polarization at the interface. The dynamical effects in the image charge force were already investigated by the authors of [25] in the case of a metal plane interface. They found that dynamical corrections become nonnegligible when the velocity v of the moving charge approaches the Fermi velocity of electrons in metals. The reason is that the image charge follows the mirror trajectory but is retarded by a distance vt_r due to the finite response time, t_r of the electron gas. Similar findings are presented by Tőkési *et al.* [18] where they studied the dynamical correction of the image force in the case of a cylindrical conducting interface. We will, in this section, investigate the image charge force for a moving ion approaching a dielectric plane and cylindrical interface and evaluate in how far dynamical corrections modify the static image force in the case of keV ions.

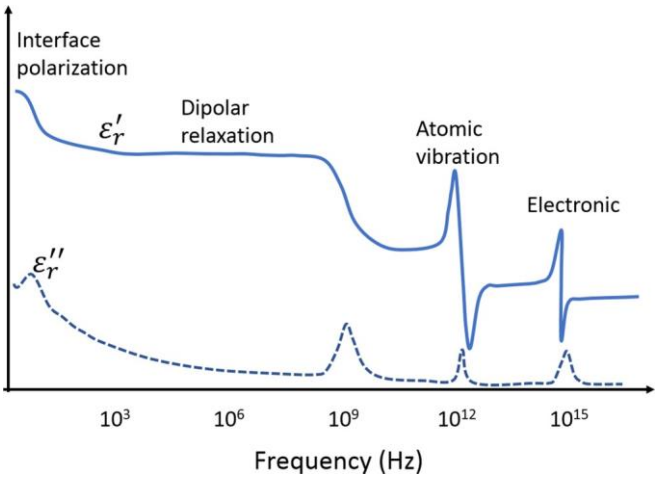

FIG. 7. Arbitrary dielectric permittivity spectrum over a wide range of frequencies. The real $\varepsilon_r^{\mathrm{r}}$ and imaginary $\varepsilon_r^{\mathrm{rr}}$ parts of permittivity are shown and various processes are labeled: Interface polarization, dipolar relaxation, atomic, and electronic resonances at higher frequencies.

A. Frequency-dependent relative permittivity

The relative permittivity of bulk describes the ability to polarize a material subjected to an electrical field. In dielectrics, this polarization originates from a number of sources: the electron cloud displaced relative to the nucleus, the relative displacement of atoms, the alignment of dipoles in the electric field, and the accumulation of charge carriers at the interface. These sources have different response times so that the relative permittivity $\varepsilon_r \equiv \varepsilon_r(\omega)$ depends on the angular frequency ω of the external electric field. We assume that the dependence of ε_r on the wave vector k can be neglected if the spatial extension of the induced dipole moments is small compared to the wavelength $2\pi/k$, which is the case for frequencies of the electromagnetic field well below optical frequencies [26]. The function $\varepsilon_r = \varepsilon_r^{\mathrm{r}} + i\varepsilon_r^{\mathrm{rr}}$ is a complex quantity and the frequency dependence of the real and imaginary parts of ε_r is illustrated in Fig. 7.

For a keV ion moving along the interface, the electric field generated at a point of the interface may quickly evolve in time. If the response time of the dielectric function is too low, the patch of induced surface charges may trail the ion, which results in a reduction of the image charge force. Only polarization sources that have a sufficiently fast response time will contribute significantly to the image charge force. For a dielectric interface, the image force is thus expected to depend on the velocity of the ion [18,25]. Considering a keV ion having typically a velocity of about 10^5 m/s and located 10 nm from the interface, the electric field generated by the ion at a point of the interface has a characteristic frequency of $v/x_p = 10$ THz, which is well in the infrared domain, where

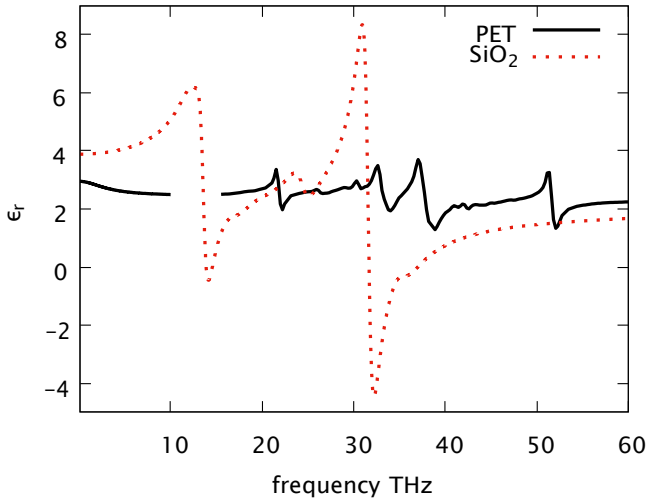

FIG. 8. Real part of the dielectric response function of SiO_2 (red dashed line) and PET (black full line) extracted from [27] and [22,28,29], respectively.

the dielectric response of insulators may vary significantly. In Fig. 8 we give the real part of the dielectric response of SiO_2 and PET insulators in the THz domain. Data were extracted from [27–29] and show that the atomic dipole resonances responsible for a large part of the value of ϵ_e are found above 10 THz.

B. Velocity-dependent image charge force

We will now evaluate the influence of the velocity of a moving charge on the image force. In a first step, we investigate the image force in the case of an infinite plane interface, which yields for the velocity-dependent image force a handy expression, facilitating the discussion. Then we check its effect on in the case of a cylindrical interface.

1. Case of an infinite plane interface

Let us consider a homogeneous dielectric which fills the region $z < 0$. The region $z > 0$ is empty. A projectile of charge q is situated at $z = z_p > 0$ and moves along the Oz coordinate with the velocity $v > 0$. The expression of the image charge force acting on a moving ion is detailed in Appendix A2 and is given by

$$F_z(z_p, v) = \frac{q^2}{2\pi\epsilon_0 v^2} \int_{-\infty}^{\infty} \frac{d\omega}{2\pi} \frac{\epsilon_r(\omega) - 1}{\epsilon_r(\omega) + 1} \frac{2z_p|\omega|}{v} K_1\left(\frac{2z_p|\omega|}{v}\right). \quad (11)$$

The image charge force depends on the velocity v of the ion and on the frequency response of the dielectric function $\epsilon_r(\omega)$. For angular frequencies $\omega \gg v/(2z_p)$, the modified Bessel function $K_1(2\omega z_p/v)$ decreases as $\exp(-2\omega z_p/v)$, so that the ratio $v/(2z_p)$ can be regarded as a cutoff angular frequency and only angular frequencies ω smaller than $v/(2z_p)$ will contribute significantly to the image charge force. For example, 7-keV Ne^{7+} ions (as used by Sahana *et al.* [4]) positioned $z_p = 10$ nm from the interface yield a cutoff angular frequency of about 10^{13} radians Hz. The latter is close to the atomic polarization resonances, where the dielectric function varies

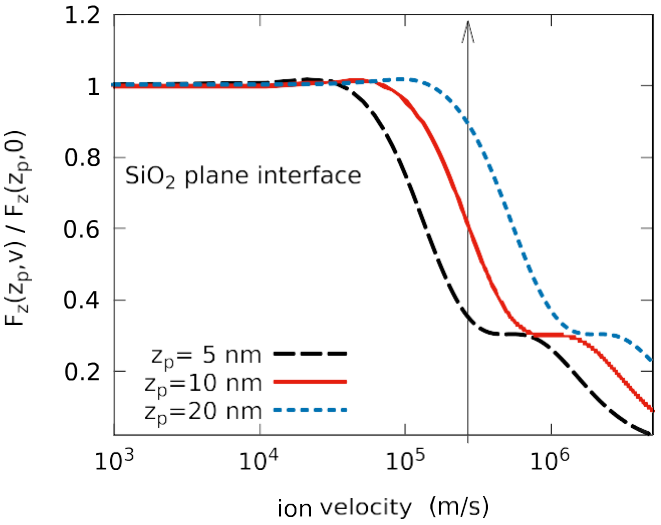

FIG. 9. Normalized image charge force $F_z(z_p, v)/F_z(z_p, 0)$ as a function of the ion velocity v, for three different distances z_p from the SiO_2 interface, $z_p = 5$, 10, and 20 nm. The arrow indicates the velocity of 7 keV Ne^{7+} ions as used by Sahana *et al.* [4].

quickly. Thus, for keV ions, the dielectric response function cannot be assumed constant and the image charge force is expected to depend significantly on the ion velocity.

For much lower ion velocities, the cutoff frequency $v/(2z_p)$ may fall below 1 Mhz. In this low-frequency range, the relative permittivity of insulators is usually constant, interfacial polarization apart. Taking $\epsilon_r(\omega) = \epsilon_r$ and integrating over ω yields the well-known image charge force for a plane vacuum-dielectric interface [30]

$$F_z(z_p, v \to 0) = \frac{q^2}{4\pi\epsilon_0} \frac{\epsilon_r - 1}{\epsilon_r + 1} \frac{1}{(2z_p)^2}. \quad (12)$$

Equation (12) can thus be seen as the adiabatic limit of Eq. (11), i.e., for of vanishingly small ion velocities v.

The dependence of the image charge force on the ion velocity is shown in Fig. 9. For better readability, we normalize the latter with respect to the adiabatic ($v \to 0$) image charge force [Eq. (12)], which allows to highlight the influence of the ion velocity on the force. The normalized force is shown for three different distances z_p from the dielectric plane interface, namely, $z_p = 5$, 10, and 20 nm. Here we used the dielectric response function $\epsilon_r(\omega)$ of SiO_2 as shown in Fig. 8, which has a large response in the THz domain due to the ionic and atomic vibrations of the glassy network. For a distance $z_p = 10$ nm from the interface, the normalized image charge force is reduced by 40% for ion velocities larger than 10^5 m/s. The reason is that for $v > 10^5$ m/s, atomic and ionic modes that usually lie in the THz range do not respond quickly enough to the time-varying electric field. Only bound electrons respond quickly enough and contribute to the surface polarization. For even larger velocities $v > 10^7$, bound electrons are not responding fast enough and the image force tends to zero. With this example we illustrate that the image charge force acting on a charge moving along a cylindrical interface is significantly reduced for velocities above a critical value, which

depends on the frequency response of the dielectric function and distance z_p from the dielectric interface.

2. Case of an infinite cylindrical interface

In the next step, we consider an infinite cylindrical interface of radius R having its symmetry axis along Oz. The interface separates the inner vacuum from the outer insulating medium of dielectric permittivity $\varepsilon_r(\omega)$. This is assumed to be complex-valued and depending on the frequency. Let a charge q move in the xOz plane with the velocity $v\underline{u}_z$, so that its time-dependent position is given by the vector $(\rho, 0, vt)$, with $\rho < R$. The expression of the dynamical image force is similar to the static one [Eq. (1)], but now takes explicitly into account the dielectric response and depends on the velocity v,

$$F_{\rm im}(\rho, v) = \frac{q^2}{16\pi\epsilon_0} \sum_{m=0}^{\infty} \int_0^{\infty} dk \frac{\partial I_m^2(k\rho)}{\partial \rho} A_m[kR, \varepsilon_r(kv)]. \tag{13}$$

The function $I_m()$ and $K_m()$ are the modified Bessel functions and $A_m()$ is a dimensionless function depending on the dielectric permittivity $\varepsilon_r(\omega)$, evaluated at the pulsation $\omega = kv$,

$$A_m[kR, \varepsilon_r(kv)] = \frac{\varepsilon_r(kv) - 1}{\varepsilon_r(kv)\frac{I_m(kR)}{K_m(kR)} - \frac{I_m'(kR)}{K_m'(kR)}}. \tag{14}$$

Here I_m' and K_m' are the partial derivatives of the Bessel functions with respect to ρ. Note that the imaginary part of A_m cancels so that A_m is real-valued. In the case of the adiabatic limit $v \to 0$, the functions $A_m()$ are evaluated using for the relative permittivity its static limit $\varepsilon_r(kv \to 0) = \varepsilon_r$, yielding expression (1).

IV. INFLUENCE OF THE ION VELOCITY ON THE THEORETICAL TRANSMITTED FRACTION

A. Image force for keV ions in SiO_2 and PET nanocapillaries

We may now check in how far the velocities of keV ions reduce the image charge force for those cases highlighted in Sec. II C, namely, for 7 keV Ne^{7+} ions through SiO_2 nanocapillaries and 3 keV Ne^{7+} ions through PET nanocapillaries. The dielectric response functions of SiO_2 nanolayers and of a thin samples of PET are pictured in Fig. 8. We compute for each case the image force as a function of ρ and for three different velocities, namely, 0.2×10^5 m/s, 1.8×10^5 m/s, and 2.8×10^5 m/s. The two later terms correspond to Ne^{7+} at 3 keV, as used by Stolterfoht *et al.* [15,16] and Ne^{7+} at 7 keV ions, as used by Sahana *et al.* [4], respectively. The first, smaller velocity is added for comparison. Expression (13) is evaluated numerically using MATHEMATICA [31] for the case of a cylindrical interface of radius $R = 50$ nm. The sum over m was limited to the 100 first angular multipoles. The results are shown in Fig. 10, where the dynamical image force $F_{\rm im}(v)$ is normalized with respect to the static one $F_{\rm im}(v = 0)$. In the case of a SIO_2 interface and 7 keV Ne^{7+} (red triangles, upper panel $v = 2.8 \times 10^5$ m/s), the dynamical image force is reduced by up to a factor of 3 compared to the adiabatic image force when approaching the interface. Indeed, for such a velocity, the response time of the first Lorentz oscillator with

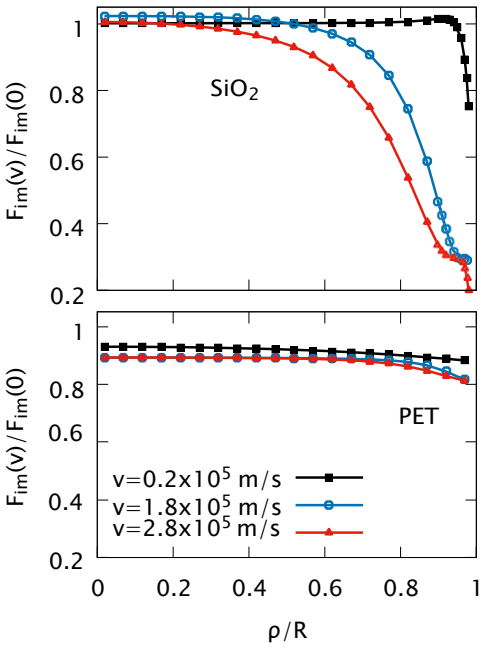

FIG. 10. Normalized image charge force, $F_{\rm im}(\rho, v)/F_{\rm im}^0(\rho)$ of a moving charge inside a cylindrical dielectric interface of radius $R = 50$ nm as a function of the dimensionless radial distance ρ/R for three different velocities, namely, $v = 2 \times 10^4$, $v = 1.8 \times 10^5$, and $v = 2.8 \times 10^5$ m/s. Upper panel: dielectric response function of SiO_2 as given in Fig. 8 is used. Bottom panel: dielectric response function of PET as given in Fig. 8 is used.

an eigenfrequency about 12 THz is too low to contribute efficiently to the image force. This results in a significant decrease of the image force when the ion approaches the interface $\rho/R \geq 0.6$, which, for $R = 50$ nm, gives a distance of about <23 nm from the interface. On the contrary, for a ten times smaller ion velocity (black squares), all the dipole oscillators follow the ion in phase and the dynamical corrections on the image force are negligible.

For a PET interface, the ratio $F_{\rm im}(v)/F_{\rm im}(0)$ for a moving charge of 1.8×10^5 is about 0.88 and mainly independent on the radial coordinate ρ. This is due to the fact that the dynamical corrections to the image force come from the finite response time of dipole alignment in PET, as indicated by the small decrease of ε_r from 3 to 2.6 in the sub 3 THz domain, as shown in Fig 8 and reported by [28]. Also, the first resonance frequency of atomic dipoles in PET lies well above 20 THz and also has a smaller strength than the first resonance in SiO_2. As a result, the dynamical image force for charges moving with a velocity up to 2.8×10^5 is only slightly affected when approaching the PET interface. We deduce that for keV ions approaching a PET interface, the dynamical corrections are small and the dielectric permittivity of PET is thus well approached by a dielectric constant $\varepsilon(f = 3\text{THz}) = 2.6$.

B. New theoretical transmitted fraction

We may now check to what extent the dynamical corrections to the static image force lifts the discrepancy found between the experimentally observed and theoretically evaluated transmitted fraction, as described in Sec. II C. Again we

solve Eq. (7), but this time using the image force as given in Fig. 10. We look for the largest initial value of $\rho_0^{\max}$ for with 7 keV Ne^{7+} ions are transmitted through SiO_2 nanocapillaries, as those used by Sahana *et al.* This time we obtain a theoretical transmitted fraction of 0.3%, only slightly larger than the 0.2% obtained previously using the static image force, but still well below the observed 20% transmission.

Similarly, for 3 keV Ne^{7+} ions through PET nanocapillaries, as those used by Stolterfoht *et al.* [15,16], dynamical corrections only negligibly increase the theoretical transmitted fraction. With respect to the one obtained with a static image force, f_{theo} increases only slightly, from 27% to 28%, which is still almost a factor of 2 lower than the observed 50% transmission. Thus we get the unfortunate result that dynamical effects do not significantly alter the theoretical transmitted fraction with respect to the static one. Even if the velocity of the keV ion is taken into account in the evaluation of the image force inside a dielectric cylinder, we are not able to explain the experimentally observed transmission fractions of ions through large-aspect nanocapillaries, especially for inner diameters of about 100 nm. Thus it seems that the discrepancy hides a phenomenon we did not yet tackle.

V. CONCLUSION

We evaluated the theoretically transmitted ion beam fraction through straight insulating nanocapillaries by calculating the fraction of ion trajectories that were not intercepted by the capillary wall. We checked via simulations that the only nonnegligible force acting on the ions was the image charge force due to the induced polarization at the inner dielectric interface of a straight cylindrical capillary. Instead of using the exact expression of the image force, we proposed a computationally faster formula that approaches very well the image force in the adiabatic limit. The transmitted fraction was evaluated in the ideal case of a monokinetic divergence free beam injected at zero tilt angle. When comparing the theoretically transmitted fraction to the three experimental data available in the literature, we found large discrepancies in the transmitted fractions. We took into account in the theory a gold collar of about 20 nm that reduces the inlet or outlet diameters of the capillaries. We found that the collar did increase the theoretically transmitted fractions by a notable amount, but did not succeed to lift the disagreement.

As the relative permittivity of a dielectric material depends on the frequency of the applied electric field, the surface polarization induced by a charge moving along the interface depended on its velocity. Thus we evaluated the image charge for a charge moving along a dielectric plane and along a dielectric cylindrical interface and, in particular, for SiO_2 and PET interfaces. We found that, for keV ions having typically a velocity about 10^6 m/s, the image charge force is controlled by the near-infrared domain (THz) of the dielectric response function. For a SiO_2 interface, the velocity of the ions affects notably the image force when the ion is close to the interface. For the PET interface, the dynamical effects of the image force are negligible in the chosen keV range.

We then checked in how far the theoretically transmitted fractions are modified when using the velocity-dependent image charge force instead of the static (adiabatic) one. The calculations were performed for 7 keV and 3 keV Ne^{7+} ions. We found that the newly calculated transmitted fractions were only slightly larger than those found previously in the case of adiabatic limit and still disagreed with the experimental results. We thus concluded that a velocity-dependent image charge force was not able to lift the highlighted disagreement. Because the electric field inside the capillary due to the accumulated charge in the walls can be neglected for large aspect-ratio capillaries, there is still no convincing explanation for why the theoretical transmitted fraction was found well below the observed one, especially for capillaries with inner diameters below 200 nm. Of course there is always this uncertainty about the real diameter of the capillary in the experimental data because of the unknown thickness of the gold collar at the inlet and outlet of the capillaries. However, how much it affects the transmitted fraction needs additional investigation.

With this work we hope to motivate new experimental work on the ion transmission through insulating nanocapillaries of different sections. We think that new data will guide authors to model more accurately the image force of keV ions trough capillaries, shedding new light on the phenomenon.

ACKNOWLEDGMENT

The author would like to thank Benoit Gervais of the Centre de Recherche sur les Ions, les Matériaux et la Photonique (CIMAP), F-14000 Caen, France, for his valuable suggestions.

APPENDIX

1. Electric field of the deposited charges versus image force on ion trajectories

We simulated the trajectories of 7-keV Ne^{7+} ions through an insulating SiO_2 nanocapillary embedded in semiconducting silicon. The inner radius of the capillary tube is 60 nm, the outer radius is 150 nm, and the length is 25 μm. The forces acting on the ions are the image force expressed by Eq. (6) and the Coulomb force due to accumulated charges at the inner capillary surface. The beam axis is aligned with the capillary axis and the injected beam intensity is 10 ions per second, thus about 10^{-17} A. The outer surface is grounded and accounts for the grounded semi-conducting Si bulk. This system model aims at modeling closely the experiment described in [4]. The bulk conductivity κ of SiO_2 is field dependent and given by the nonlinear Poole-Frenkel relation [32,33]

$$\kappa(E) = \kappa_0 \exp(\sqrt{E/E_c}). \tag{A1}$$

The field-independent bulk conductivity κ_0 is set to 10^{-15} S/m [34] and the critical field E_c is set be 10^8 V/m, which is the typical range where the conductivity SiO_2 becomes nonlinear [17,33]. We show in Fig. 11 the computed ion trajectories. The accumulated charge in the capillary wall is shown by the red curves. After about 3 hours, the deposited charge per unit time is balanced by the leakage current and the accumulated charge has reached its asymptotic distribution. The electric field inside the capillary wall reaches at that moment 30 MV/m, putting the conductivity well within the nonlinear regime. The transmitted beam fraction as a function of time is

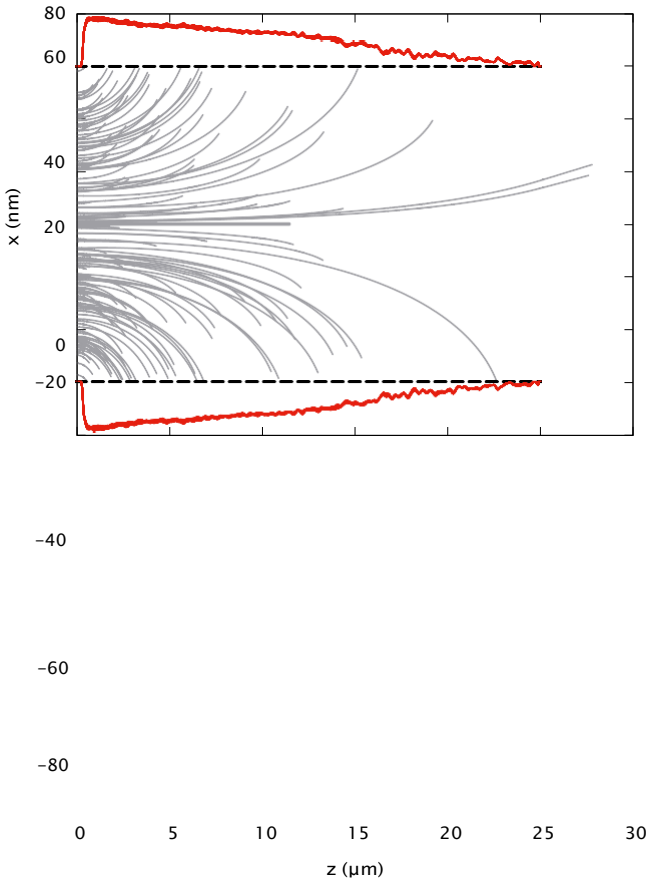

FIG. 11. Simulated ion trajectories (gray curves) through a 25-μm-long nanocapillary of inner radius of 60 nm, as indicated by

Let $\tilde{E}_x^q$ be the Fourier transform in the frequency domain of the electric field E_x^q,

$$\tilde{E}_x^q(\omega, x_p, y, z, v) = \frac{-q}{4\pi\epsilon_0}\int_{-\infty}^{\infty} \frac{x_p e^{i\omega t}\,dt}{\left(x_p^2 + y^2 + (z - vt)^2\right)^{3/2}} = -\frac{q}{2\pi\epsilon_0 v^2}\,\frac{|\omega|}{\gamma}\,K_1\!\left(\frac{|\omega|\sqrt{x_p^2+y^2}}{\gamma v}\right) e^{i\omega z/v} \equiv G(\omega, x_p, y, v)\, e^{i\omega z/v}, \tag{A6}$$

where $K_1()$ is the modified Bessel function of order 1.

In the following we assume that the dielectric function is local in space so that $\varepsilon_r(\omega, k) \approx \varepsilon_r(\omega)$. This assumption is valid for $k \ll \pi/a$, where $a \approx 0.5$ nm is the typical length of the molecules responsible for the polarization. Using Eq. (A5) we have, at both sides of the interface $x = 0$,

$$\tilde{D}^{-}(\omega, y, z, v) = \varepsilon_0(\omega)\,\frac{\tilde{\sigma}(\omega, y, z, v)}{2} + \varepsilon_0\tilde{E}^{-}(), \tag{A7}$$

x x

p

x

$2\varepsilon_0$

the black dashed line. The red curves indicate the accumulated charge x in arbitrary units at the inner interface.

=

$$\tilde{\sigma}^{r}(\omega, y, z, v) \quad \tilde{\rho}^{0}(x, 2)$$

$$D_x^+(\omega, y, z, v) = \quad - \qquad \quad + \varepsilon_0 E_x() \quad . \qquad \text{(A8)}$$

2

electric field due to the deposited charges is removed so as to put into evidence the zero effect of the deposited charge on the transmission.

2. Image charge at plane interface

Let us consider a homogeneous dielectric of relative per-

Using the interface condition

$$\tilde{D}^{-}(\omega, x, y, v) = \tilde{D}^{+}(\omega, x, y, v),$$

we obtain the expression for $\sigma(\omega, y, z, v)$,

$$-qe^{iwz/v}\ \varepsilon\ (\omega) - 1\ |\omega|$$

mit ty ε_r which fills the region $x < 0$. The region $x > 0$ is

$$\tilde{\sigma}(\omega, y, z, v) = \quad _r \quad G(\omega, x_p, y, v). \quad \text{(A9)}$$

tivi

$$\Pi \quad \varepsilon_r(\omega) + 1 \; v^2$$

1

$$\frac{q}{} \int_{-\infty}^{\infty} \frac{d\omega}{} \int \int e^{-i\omega t} x \, \tilde{\sigma}(\omega, y, z, v) dz$$

$z_p = vt$. The x component of the electric field at the interface

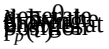

$$E^q(x\ ,y,z,t) = \frac{q\qquad\qquad -x_p\qquad\qquad}{}. \qquad \text{(A2)}$$

$$\frac{x^2 + y^2}{(z \mp vt)^{2}}^{3/2} \quad (A10)$$

$$x \quad p \qquad 4\pi\epsilon_0 \left(x^2 + y^2 + (z - vt)^2\right)^{2/3}$$

Integration over z gives

$$\int_{d\omega}^{\infty}$$

747

ε_r

at

th

e

in

te

rf

a

c

e

x

=

0,

th

e

el

e

ct

ri

c

fi

el

d

E

q

in

d

u

c

es

at

th

$$F_x(x_p) = \frac{}{2}$$

e

Π

$^2\varepsilon_0 v$

3

∞

2

Π

$|\omega|$

ε_r

(ω

)

1

by the surface charges σ at the dielectric side $x = 0^-$ is $-\frac{\sigma}{2}$ $\int_{\infty}$

but $+\frac{\sigma}{}$ at $x = 0^+$

$\times$

$-\infty$

reads

$$E_x^- = E_x^q - \frac{\sigma}{2\varepsilon_0}, \quad x = 0^-, \tag{A3}$$

while in the empty region side $x = 0^+$ it reads

$$E_x^+ = E_x^q + \frac{\sigma}{2\varepsilon_0}, \quad x = 0^+. \tag{A4}$$

In the absence of free surface charges, the x component of the displacement field D_x is continuous across the interface. The relation between $D = \varepsilon E$ is nonlocal in time and position and is more comfortably used in the frequency and wave-number domain. The later relation is more convenient when expressed in the Fourier space, where it simplifies to

$$\tilde{D}(k, w) = \tilde{\varepsilon}(k, \omega)\tilde{E}(q, \omega), \tag{A5}$$

Noting that

$$\int_{-\infty}^{\infty} dy G(x\ y)^2 = \pi \frac{v}{|\omega|} K\left(\frac{2x_p|\omega|}{v}\right), \tag{A12}$$

we have

$$F_x(x_p) = \frac{-q^2}{2\pi\varepsilon_0 v^2} \int_{-\infty}^{\infty} \frac{d\omega}{2\pi} |\omega| \frac{\varepsilon_r(\omega) - 1}{\varepsilon_r(\omega) + 1} K\left(\frac{2x_p|\omega|}{v}\right). \tag{A13}$$

3. Image force for a spherical dielectric interface

Assume a spherical cavity of radius R 1 in a dielectric bulk of dielectric constant $\varepsilon_r > 1$. A charge q is located inside the cavity at a distance $x < 1$ from the center of the sphere.

The image potential at x is given by [35]

$$V_{\rm im}^{\rm sph}(x) = \frac{-q}{4\pi\varepsilon_0}\frac{\varepsilon_r - 1}{\varepsilon_r + 1}\sum_{n=0}\frac{(n+1)x^{2n}}{n+1-\delta}, \tag{A14}$$

where $\delta = \frac{1}{\varepsilon_r+1} < \frac{1}{2}$. To simplify the notation, we define

$$q^r = \frac{-q}{4\pi\varepsilon_0}\frac{\varepsilon_r - 1}{\varepsilon_r + 1}.$$

Noting that $(1-\frac{\delta}{(n+1)})^{-1} = 1 + \frac{\delta}{(n+1)} + \frac{\delta^2}{(n+1)^2} + \ldots$, we may expand the image potential is powers of δ,

$$V_{\rm im}^{\rm sph}(x) = q^r\sum_{n=0}\frac{x^{2n}}{1-\frac{\delta}{n+1}} = q^r\sum_{n=0}\left[x^{2n} + \delta\frac{x^{2n}}{n+1} + \delta^2\frac{x^{2n}}{(n+1)^2} + \ldots\right]. \tag{A15}$$

The terms on the right-hand side become smaller with increasing power of δ, so that the zero-order term is the leading term of the image potential. Noting the closed form

$$\sum_{n=0}x^{2n} = \frac{1}{1-x^2}, \tag{A16}$$

we get

$$V_{\rm im}^{\rm sph}(x) = q^r\frac{1}{1-x^2} + O(\delta). \tag{A17}$$

The zero-order term in the δ expansion of the image force is eventually

$$F_{\rm im}^{\circ} = \frac{q}{4\pi\varepsilon_0}\frac{\varepsilon_r - 1}{\varepsilon_r + 1}\frac{x}{(1-x^2)^2}. \tag{A18}$$

[1] N. Stolterfoht, J.-H. Bremer, V. Hoffmann, R. Hellhammer, D. Fink, A. Petrov, and B. Sulik, Transmission of 3 keV Ne^{7+} Ions through Nanocapillaries Etched in Polymer Foils: Evidence for Capillary Guiding, Phys. Rev. Lett. **88**, 133201 (2002).

[2] T. Ikeda, Y. Kanai, T. M. Kojima, Y. Iwai, T. Kambara, Y. Yamazaki, M. Hoshino, T. Nebiki, and T. Narusawa, Production of a microbeam of slow highly charged ions with a tapered glass capillary, Appl. Phys. Lett. **89**, 163502 (2006).

[3] K. Schiessl, W. Palfinger, K. Tőkési, H. Nowotny, C. Lemell, and J. Burgdörfer, Simulation of guiding of multiply charged projectiles through insulating capillaries, Phys. Rev. A **72**, 062902 (2005).

[4] M. B. Sahana, P. Skog, Gy. Vikor, R. T. Rajendra Kumar, and R. Schuch, Guiding of highly charged ions by highly ordered SiO_2 nanocapillaries, Phys. Rev. A **73**, 040901(R) (2006).

[5] C. Lemell, J. Burgdörfer, and F. Aumayr, Interaction of charged particles with insulating capillary targets - The guiding effect, Prog. Surf. Sci. **88**, 237 (2013).

[6] N. Stolterfoht and Y. Yamazaki, Guiding of charged particles through capillaries in insulating materials, Phys. Rep. **629**, 1 (2016).

[7] N. Stolterfoht, Simulation and analysis of ion guiding through a nanocapillary in insulating polymers, Phys. Rev. A **87**, 012902 (2013).

[8] N. Stolterfoht, Simulations of ion-guiding through insulating nanocapillaries of varying diameter: Interpretation of experimental results, Atoms **8**, 48 (2020).

[9] E. Giglio, Charge relaxation rates in insulating straight capillaries, Phys. Rev.A **101**, 052707 (2020).

[10] E. Giglio, S. Guillous, and A. Cassimi, Ion-beam focusing by self-organized axis-symmetric potentials in insulating capillaries, Phys. Rev.A **98**, 052704 (2018).

[11] E. Giglio and T. Le Cornu, Effect of secondary electrons on the patch formation in insulating capillaries by ion beams, Phys. Rev. A **103**, 032825 (2021).

[12] K. Schiessl, W. Palfinger, K. Tőkési, H. Nowotny, C. Lemell, and J. Burgdörfer, Simulation of ion guiding through insulating capillaries: Effects of inter-capillary interaction, Nucl. Instrum. Methods Phys. Res., Sect. B **258**, 150 (2007).

[13] H. Q. Zhang, N. Akram, and R. Schuch, Transmission of highly charged ions through mica nanocapillaries of rectangular cross-section, Nucl. Instrum. Methods B **408**, 61 (2017).

[14] H. Q. Zhang, N. Akram, P. Skog, I. L. Soroka, C. Trautmann, and R. Schuch, Tailoring of keV-Ion Beams by Image Charge when Transmitting through Rhombic and Rectangular Shaped Nanocapillaries, Phys. Rev. Lett. **108**, 193202 (2012).

[15] N. Stolterfoht, R. Hellhammer, Z. Juhász, B. Sulik, E. Bodewits, H. M. Dang, and R. Hoekstra, Guided transmission of 3-keV Ne^{7+} ions through nanocapillaries in insulating polymers: Dependence on the capillary diameter, Phys. Rev. A **82**, 052902 (2010).

[16] N. Stolterfoht, Z. Juhász, P. Herczku, S. T. S. Kovécs, R. Rácz, S. Biri, C. Cserháti, and B. Sulik, Transmission of 3-keV Ne^{7+} ion through nanocapillaries probing the discharge process, Eur. Phys. J. D **75**, 136 (2021).

[17] P. Dash, M. Yuan, J. Gao, E. Furman, and M. T. Lanagan, High electric field conduction in low-alkali boroaluminosilicate glass, J. Appl. Phys. **123**, 054102 (2018).

[18] K. Tőkési, L. Wirtz, C. Lemell, and J. Burgdörfer, Hollow-ion formation in microcapillaries, Phys. Rev.A **64**, 042902 (2001).

[19] K. Tőkési, L. Wirtz, C. Lemell, and J. Burgdörfer, Interaction of highly charged ions with microcapillaries, Nucl. Instrum. Methods Phys. Res. Sect. B **154**, 307 (1999).

[20] S. T. Cui, Electrostatic potential in cylindrical dielectric media using the image charge method, Mol. Phys. **104**, 2993 (2006).

[21] J. D. Jackson, Point charge near a conducting sphere at fixed potential, in *Classical Electrodynamics*, 3rd ed., Sec. 2.4 (John Wiley and Sons, New York, 1963), p. 150.

[22] Y.-S. Jin, G.-J. Kim, S.-G. Jeon, Terahertz dielectric properties of polymers, J. Korean Phys. Soc. **49**, 513 (2006).

[23] R. Kitamura, L. Pilon, and M. Jonaszn, Optical constants of silica glass from extreme ultraviolet to far infrared at near room temperature, Appl. Opt. **46**, 8118 (2007).

[24] G.-Y. Liu, W.-F. Sun, and Q.-Q. Lei, Charge injection and dielectric characteristics of polyethylene terephthalate based on semiconductor electrodes, Materials **14**, 1344 (2021).

[25] J. Harris and R. O. Jones, Image force for a moving charge, J. Phys. C: Solid State Phys. **7**, 3751 (1974).

[26] J. Petzelt and I. Rychetský, Dielectric function, *Encyclopedia of Condensed Matter Physics* (Elsevier, Amsterdam, 2005), p. 426.

[27] G. Cataldo, E. J. Wollack, A. D. Brown, and K. H. Miller, Infrared dielectric properties of low-stress silicon oxid, Opt. Lett. **41**, 1364 (2016).

[28] E. V. Fedulova, M. M. Nazarov, A. A. Angeluts, M. S. Kitai, **V.** I. Sokolov, and A. P. Shkurinov, *Proceedings of SPIE*, Vol. 8337, *Saratov Fall Meeting 2011: Optical Technologies in Biophysics and Medicine XIII, 28 February 2012* (SPIE, Bellingham, WA, 2012), p. 83370I.

[29] X. Zhang, J. Qiu, J. Zhao, X. Li, and L. Liu, Complex refractive indices measurements of polymers in infrared bands, J. Quant. Spectrosc. Radiat. Transfer **252**, 107063 (2020).

[30] J. D. Jackson, *Classical Electrodynamics*, 3rd ed. (John Wiley and Sons, New York, 1999).

[31] Wolfram Research, Inc., MATHEMATICA, Version 7.0, Champaign, IL (2008).

[32] J. Frenkel, On pre-breakdown phenomena in insulators and electronic semi-conductors, Phys. Rev. **54**, 647 (1938).

[33] S.K. Gupta, A. Azam, and J. Akhtar, Experimental analysis of current conduction through thermally grown SiO_2 on thick epitaxial 4H-SiC employing Poole-Frenkel mechanism, Pramana J. Phys. **74**, 325 (2010).

[34] J. K. Srivastava, M. Prasad, and J. B. Wagner Jr., Electrical conductivity of silicon dioxide thermally grown on silicon, J. Electrochem. Soc. **132**, 955 (1985).

[35] D. V. Redzić, M. S. A. Eldakli, and M. D. Redzić, Image charge inclusion in the dielectric sphere revisited, Eur. J. Phys. **33**, 1751 (2012).